N-FINDR: an algorithm for fast autonomous spectral end-member determination in hyperspectral data,

Michael E. Winter*, Department of Earth Sciences, University of Queensland (Australia) and Technical Research Associates, Inc. (USA)

ABSTRACT

The analysis of hyperspectral data sets requires the determination of certain basis spectra called "end-members". Once these spectra are found, the image cube can be "unmixed" into the fractional abundance of each material in each pixel. There exist several techniques for accomplishing the determination of the end-members, most of which involve the intervention of a trained geologist. Often these end-members are assumed to be present in the image, in the form of pure, or unmixed, pixels. In this paper a method based upon the geometry of convex sets is proposed to find a unique set of purest pixels in an image. The technique is based on the fact that in N spectral dimensions, the N-volume contained by a simplex formed of the purest pixels is larger than any other volume formed from any other combination of pixels. The algorithm works by "inflating" a simplex inside the data, beginning with a random set of pixels. For each pixel and each end-member, the end-member is replaced with the spectrum of the pixel and the volume is recalculated. If it increases, the spectrum of the new pixel replaces that end-member. This procedure is repeated until no more replacements are done. This algorithm successfully derives end-members in a synthetic data set, and appears robust with less than perfect data. Spectral end-members have been extracted for the AVIRIS Cuprite data set which closely match reference spectra, and resulting abundance maps match published mineral maps.

Keywords: end-member, hyperspectral, autonomous

1. INTRODUCTION

Hyperspectral data represents a challenge from a data-processing point of view, as it can consist of hundreds of bands. A necessary first step is to reduce the complexity of the image by a dimensionality reduction, which compresses the image data to a few meaningful bands. The most widely used methods for reducing the dimensionality of the data are orthogonal subspace projections (OSPs) and unmixing the image based on a set of component spectra (end-members). OSPs reduce the dimensionality of the data by finding the combinations of bands, which best represent the image in some manner. While OSPs reduce dimensionality, the resulting images have a mathematical rather than physical relationship with the original image. The principal advantage of unmixing an image using end-members it that offers the reduction of the complexity of the data set based on a physical set of component spectra. The resulting images are the abundance of the corresponding substance for that pixel.

In many cases end-member spectra for an image are unknown. The image may be classified using laboratory spectra, however this requires that the image be converted to reflectance. Moreover, the selection of end-members can be non-unique. A more optimal approach is to determine the end-member spectra based solely on the information contained within the image itself.

A perfect algorithm for the determination of end-members would find end-members directly from the image regardless of composition or noise, without any *a priori* knowledge. However, due to the mathematical complexity of the problem and imperfections in any real data (the influence of atmosphere, sensor noise etc), a more realistic goal is to determine *recognizable* spectra, and produce *useful* abundance maps. Recognizable spectra allow the determination of the real end-member from a spectral library, while the abundance maps show roughly the relative amount of each end-member in each pixel.

Generally, algorithms which derive end-members directly from an image fall into two broad categories: those which assume that the end-members themselves are present in the image in the form of pure, or unmixed, pixels, and those which derive the spectra of the end-members analytically (for example "factor analysis", Harmon, 1967). Pure pixel based techniques, which include this algorithm, the selection of extreme points of an n-dimensional scatter plot, and the "convex-cone"

* Correspondence: Email: winter@shake2.earthsciences.uq.edu.au; Telephone: +61 7 3876-7319

Part of the SPIE Conference on Imaging Spectrometry V • Denver, Colorado • July 1999
SPIE Vol. 3753 • 0277-786X/99/$10.00

method (Ifarraguerri, 1997), leverage the simplification that the end-members themselves are present in the image. This allows a reduction in the scope of the problem by restricting the possible characteristics of the end-members to discrete points in spectral-feature-space.

The N-FINDR algorithm (Winter, 1999) is essentially an automated technique for finding the purest pixels in an image. The goal of the algorithm is to duplicate the successful non-automated technique of selecting extreme points of an n-dimensional scatter plot. Although this method has its critics (e.g. Craig 1990; 1994) it remains the most widely used and successfully applied method for determining end-members without *a priori* information. N-FINDR attempts to find the simplex of maximum volume that can be inscribed within the hyperspectral data set using a simple non-linear inversion. The convex nature of hyperspectral data allows this operation to be performed in a quick and relatively straightforward manner. Subsequent optimizations of the algorithm (not detailed here) have allowed the use of this algorithm at speeds approaching those required by real-time applications.

This work focuses on the performance of the algorithm on both synthetic and real data sets. To illustrate the viability of the algorithm under realistic circumstances, areal distributions of the minerals alunite, kaolinite and calcite are mapped using the AVIRIS Cuprite Nevada sample image.

2. THE ALGORITHM

Most methods of determining end-members autonomously from an image make use of the geometric nature of hyperspectral data (for example, see Craig 1994, Boardman, 1995). Data analysis problems can often be viewed geometrically, with each observation occupying a point in a space spanned by all of the data (c.f. Rawlings, 1988).

Generally, the spectra for a given pixel in an image is assumed to be a linear combination of the end-member spectra:

$$p_{ij} = \sum_k e_{ik} c_{kj} + \varepsilon \quad , \tag{1}$$

where p_{ij} is the i-th band of the j-th pixel, e_{ik} is the i-th band of the k-th end-member, c_{kj} is the mixing proportions for the j-th pixel from the k-th end-member, and ε is gaussian random error (assumed to be small). Since the pixel compositions are assumed to be percentages, the mixing proportions are should sum to one:

$$\sum_k c_{kj} = 1 \quad . \tag{2}$$

The mixing proportions can be visualized as "abundance maps" which depict the fractional composition of the end-member material as a gray level image. Any distribution of data which follows the mixture model outlined in Equations 1 and 2 forms a simplex (Lay, 1982) in data space. A simplex is the simplest geometric object which spans a given space, for example a triangle in two dimensions and a tetrahedron in three dimensions.

If $c_{kj} \approx 1$ for any end-member contribution in a pixel, the other end-member contributions must be near zero, and the pixel can be classified as pure. These pure pixels define the vertices of the N-dimensional scatter plot of the data. Moreover, these pure pixels define a simple of maximum volume which can be inscribed within the data set. This procedure "inflates" a simplex within the data set in order to determine these pixels. A necessary assumption is that there exists at least one pure pixel per end-member species within the image.

2.1 Pre-processing

In order for the volume to be determined the dimensionality of the image must be reduced to be one less than the number of end-members. This is accomplished through an orthogonal subspace projection. OSPs act to compress the information in an image based on a mathematical criteria: maximum power for the singular value decomposition (Rawlings, 1988), maximum variation for the principal components transform, and noise weighted variation for the Maximum Noise Fraction (MNF) transform (Green, 1988). In theory, the MNF transform offers the best performance, however for the purposes of this algorithm all methods appear to work equally well.

2.2 Volume determination

Let **E** be the matrix of end-members augmented with a row of ones:

$$\mathbf{E} = \begin{bmatrix} 1 & 1 & \cdots & 1 \\ \vec{e}_1 & \vec{e}_2 & \cdots & \vec{e}_l \end{bmatrix} , \tag{3}$$

where $\vec{e}_i$ is a column vector containing the spectra of end-member *i*.

The volume (V) of the simplex formed by using the end-member estimates is proportional to the determinant of **E**:

$$V(\mathbf{E}) = \frac{1}{(l-1)!} abs(|\mathbf{E}|) , \tag{4}$$

where (l - 1) is the number of dimensions occupied by the data.

2.3 Non-linear inversion

The procedure begins with a random set of pixels as end-members. In order to refine the estimate of the end-members, every pixel in the image must be evaluated as to its likelihood of being a pure or nearly pure pixel. To do this, the volume must be calculated with each pixel in place of each end-member. A trial volume is calculated for every pixel in each end-member position by replacing that end-member and recalculating the volume. If the replacement results in an increase in volume, the pixel replaces the end-member. This procedure is repeated until there are no more replacements of end-members.

This algorithm amounts to a simple non-linear inversion for the largest simplex, which can be inscribed within the data. The convex nature of hyperspectral data simplifies this inversion process, as there are no local maxima in good data. There will be local maxima in the case where the distribution of data is truncated and there are no pure pixels. For this reason, the algorithm is run several times with different sets of initial end-members and the end-member set resulting in the largest total volume is returned.

An end-member consisting of all zeros can be used as an *a priori* estimate of the "shade" end-member. This is not necessary, but can speed up the convergence of the algorithm. This is done for all the examples presented in this paper.

2.4 Unmixing

Once the pure pixels are found, their spectra can be used to unmix the original image. This produces a set of images, each of which shows the abundance for each end-member for each pixel. Here the inversion procedure used is either a least squares inversion or a non-negatively constrained inversion. Determining end-member contributions using least squares uses the solution of the normal equations (Rawlings, 1988):

$$\mathbf{C} = (\mathbf{E}^T\mathbf{E})^{-1}\mathbf{E}^T\mathbf{P} . \tag{5}$$

Where **C** is the end-member composition for pixel **P**. Non-negatively constrained least squares enforces the physical constraint that no end-member may have a negative abundance. This algorithm is too complex to detail here, but it is described by Lawson and Hanson (1974).

2.5 Discussion

The above outlined algorithm will encounter difficulties in certain circumstances. If there are no completely unmixed pixels for a certain end-member, then the algorithm will find the least mixed pixel that most closely approximates the end-member. Furthermore, if there are mixed pixels with a higher brightness than the unmixed pixels, the algorithm will select them as end-members. This inaccuracy is mitigated somewhat by the requirement that for an unmixed pixel to be selected, its brightness must increase dramatically as the spectral angle between it and the true end-member increases. Thus when the algorithm selects unmixed pixels as end-members, they tend to be at a small spectral angle from the true end-member.

It is feasible for a real image to contain no pure or nearly pure pixels. In this case, one of the basic assumptions of this algorithm is violated. The partially pure data can still be useful, as it defines an axis in spectral-feature space. The resulting end-member chosen will be a mixed pixel. Because of the convexity of the remainder of the data, the largest inscribed simplex still has vertices at the location of the pure end-members where they exist (see Figure 1). This effect can be examined further with synthetic data.

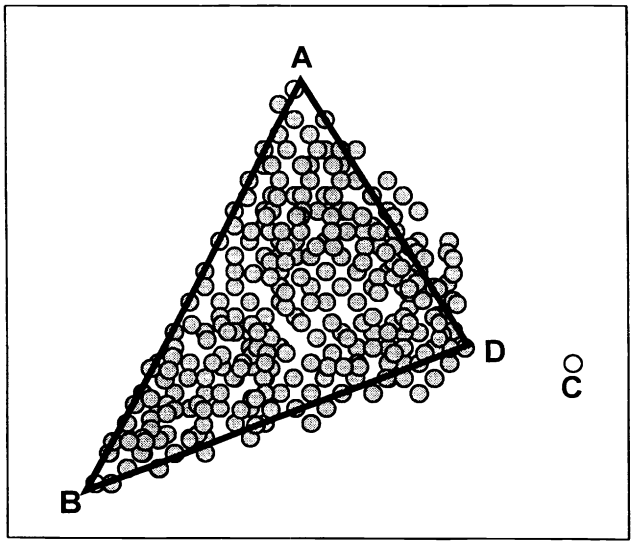

Figure 1: Points A, B, and C represent the three true end-members for an image, however due to a lack of any pure pixels of type C, the selected end-members are A, B, and D (a mixed pixel).

3. APPLICATION TO SYNTHETIC DATA

In order for an end-member determination algorithm to be considered successful, it must be provide good results on images with a wide variety of imperfections. Unfortunately, success on real data is difficult to determine as the true end-members and abundance maps are often unknown. Synthetic data is therefore useful for testing that the algorithm does indeed work. The performance of an algorithm under adverse conditions can also be examined in a controlled manner.

3.1 Synthetic image: perfect data

Synthetic abundance maps were generated for nine end-members, arranged in a grid across the image (see Figure 2). The end-member abundance decreases linearly away from the specified grid point. These abundance maps are then re-normalized so that the contributions of the end-members sum to one. Nine end-members, including one vector of all zeros (to represent shade) were derived from a 50 band short-wave infrared image of Cuprite Nevada. The actual choice of end-members is arbitrary as long as they are linearly independent, however using physical end-members results in an image that mimics the spectral characteristics of real data.

The end-members were then "mixed" based on the specified end-member abundances. The resulting image was 350 pixels by 350 pixels with 50 bands and represents a perfect case of linearly mixed data.

The above outlined algorithm was applied to this data set. The derived end-members were used to produce abundance maps using linear unmixing. The derived end-members exactly matched the input ones, and the corresponding abundance maps exactly matched the abundance maps used to generate the synthetic image. This result is perhaps not surprising, however it does show that the algorithm indeed works.

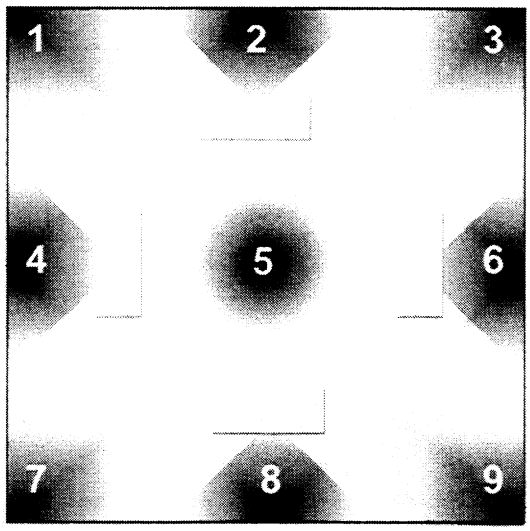

Figure 2: End-member distributions used to construct the synthetic image. End-member 5 represents shade.

3.2 Synthetic image: imperfect data

A more interesting case can be constructed which tests the robustness of the algorithm with less than perfect data. For this test, the above abundance maps were clipped, so that maps 2 though 8 had their end-member abundance limited to 0.4, with any excess being added to the shade contribution to the pixel. Abundances for end-members 1 and 9 were left as is. A synthetic image was again constructed by "mixing" the end-members and abundance maps. Abundance maps 2-8 will have no pixels which are even remotely pure, violating a fundamental assumption of this algorithm.

The N-FINDR algorithm was run on the synthetic data set and 9 end-members were derived. These were used to unmix the original synthetic image using simple linear unmixing. Several original and derived end-members are shown in Figure 3, and selected original and derived abundance maps are shown in Figure 4. Although six of the eight end-members had no pure pixels, the abundance maps, although they do contain significant negative values, still reflect the true abundance. The other abundance maps not shown also show similar success.

An encouraging feature of the algorithm is that the derived end-members 1 and 9 exactly match the input end-members. Their selection was not adversely effected by the truncated distribution of the other end-member contributions. The end-members for the other bands show mixture as would be expected.

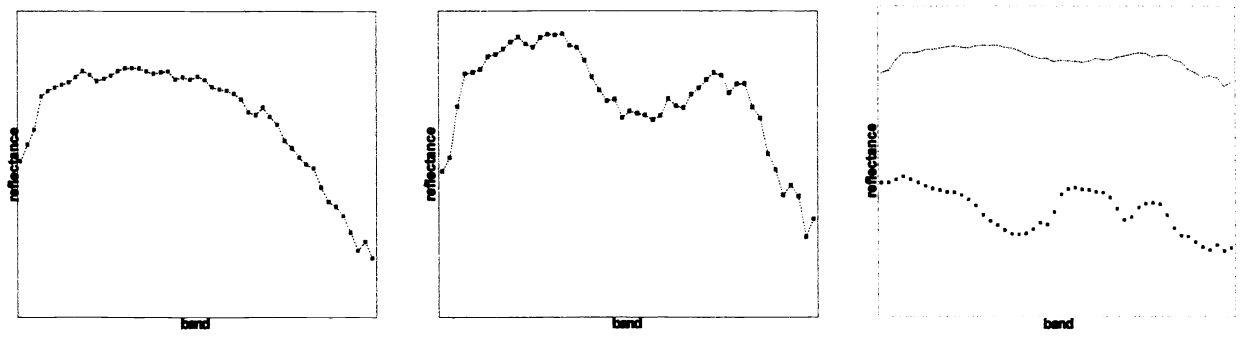

Figure 3: Original end-members (square points) and derived end-members (dashed line) for end-members 1, 9 and 2. Derived end-member spectra 1 and 9 exactly match the input end-member spectra. The end-member spectra 2, which contained no pure pixels, is incorrect.

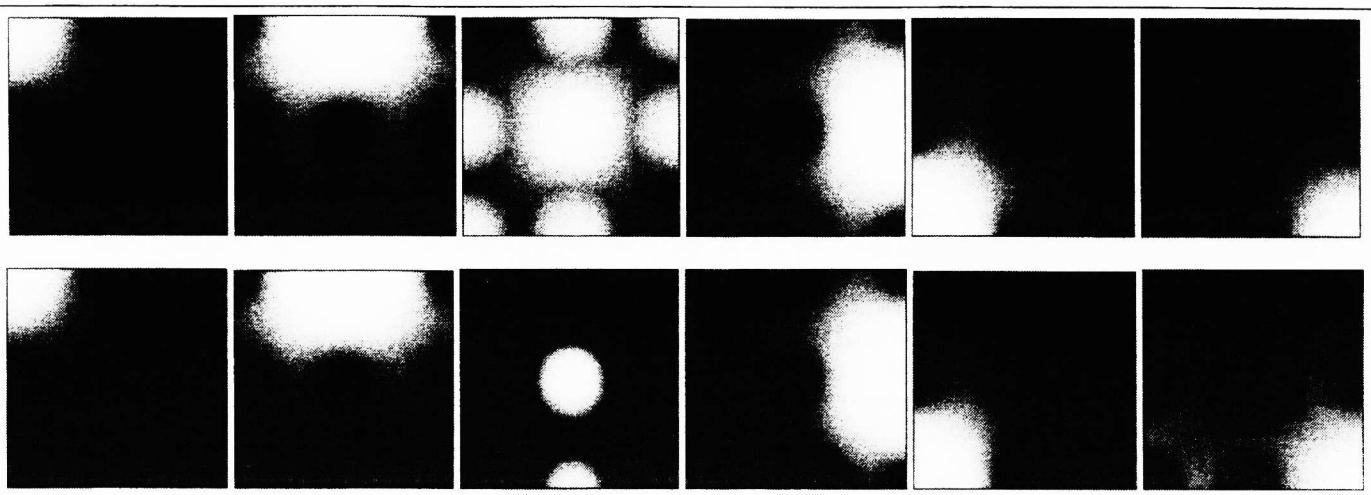

Figure 4: Top row: selected initial synthetic abundance maps used to generate the synthetic image; from left to right: end-member 1, 2, 5 (shade), 6, 7, 9. Bottom row: abundance maps found by linearly unmixing N-FINDR end-member spectra derived from the synthetic image; from left to right: end-member 1, 2, 5 (shade), 6, 7, 9. Grey scale equates to abundance of end-member in each pixel scaled to cover the range present in each abundance map. Negative end-member abundances were removed from the derived images.

4. APPLICATION TO AVIRIS CUPRITE DATA

The procedure was applied to hyperspectral data collected by the AVIRIS sensor over Cuprite, Nevada. AVIRIS is a high quality low noise hyperspectral instrument that acquires data in 224 contiguous spectral bands from 400 to 25000 nm at approximately 20 meter resolution over a swath width of 10 km (Vane, 1995). Cuprite is a mining area in southern Nevada with hydrothermally altered and unaltered rocks and little vegetation. It has been extensively used for remote sensing experiments over the past twenty years and the minerals have been extensively mapped (Ashley and Abrams, 1980).

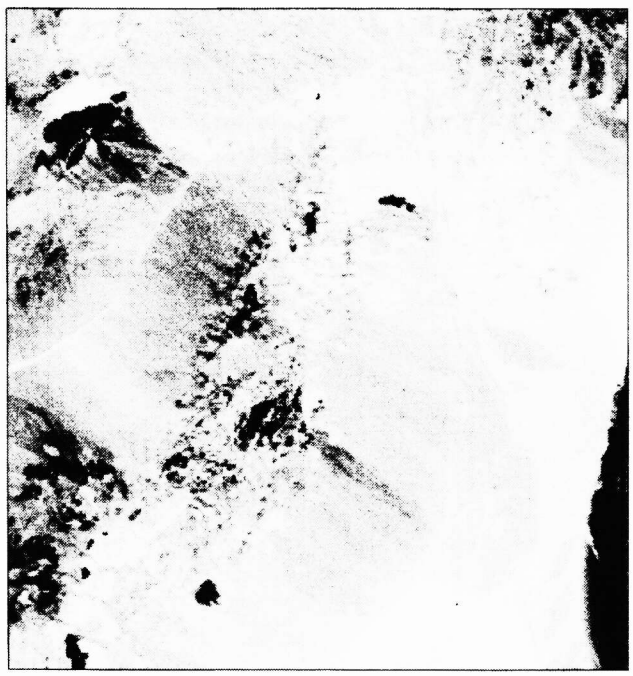

Figure 5: Broadband SWIR image of the Cuprite sample data formed by summing the fifty spectral bands used for processing.

For this experiment 50 contiguous SWIR bands (covering 1978 to 2478 nm) were selected from the 1996 AVIRIS flight. A ten by ten kilometer area (614 by 657 pixels) covering the geologically interesting parts of the AVIRIS scene was processed by the procedure discussed above. A broadband SWIR image of the selected scene is shown in Figure 5. Some of the results of the processing are shown in Figures 6 and 7. The entire procedure of end-member determination and linear unmixing was completed in less than 26 seconds on a 400 MHz Pentium II.

Determining the success of end-member determination with a real image is much more difficult than with synthetic data. In order to determine the performance of the algorithm, three approaches are used: a comparison with laboratory spectra, a comparison of derived end-member abundance maps with published results, and an examination of scatter plots of the unmixed image.

4.1 Comparison of derived end-member spectra with laboratory spectra

Three of the derived spectra are shown in Figure 6, compared with laboratory derived mineral spectra published by the US Geological Survey (Clark, 1993). The derived end-member spectra show a good resemblance to the laboratory derived spectra, especially considering the potential inaccuracies in converting the image to reflectance.

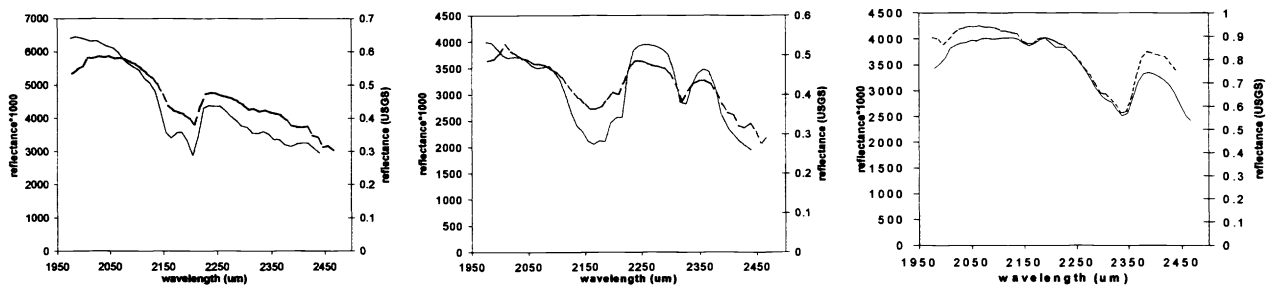

Figure 6: Three end-members derived from the cuprite scene (dashed line) compared with USGS laboratory spectra (solid line). Spectra are (from left to right): alunite, kaolinite, and calcite.

4.2 Comparison of derived end-member abundance maps with published results

The abundance maps obtained through the unmixing of the input image with the derived end-members provide a good benchmark for the end-member determination algorithm. The abundance maps obtained through non-negatively constrained linear inversion for alunite, kaolinite, and calcite are shown in Figure 7. These broadly mimic the alteration maps shown by Ashley and Abrams (1980). The alunite distribution shows a good resemblance to the alunite fraction map obtained through a different means of analysis by Resmini *et. al.* (1997).

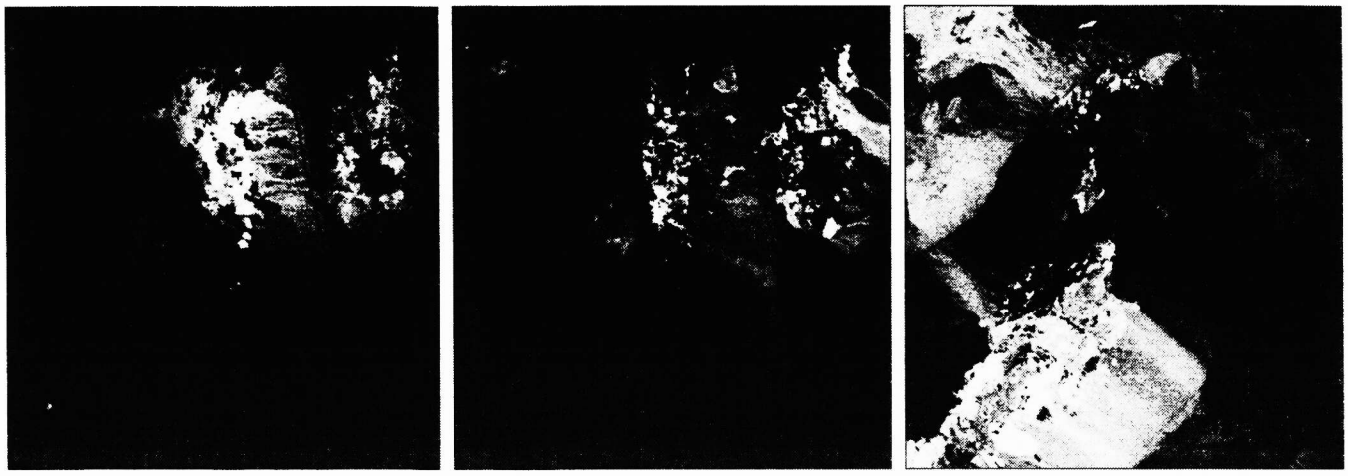

Figure 7: Abundance maps of alunite, kaolinite, and calcite derived from a non-negatively constrained unmix using the derived end-members. Brightness corresponds to greater abundance of the specified mineral.

4.3 Examination of scatter plots of the unmixed image

If the end-members are determined correctly, the simplex formed by the end-members encloses the data. In two dimensions, this is easily visualized by imagining that the three end-members form a triangle, with each pixel lying within. This concept can be generalized to higher dimensions, but the situation becomes harder to visualize. The transformation provided by linear unmixing can be used to simplify this visualization.

End-member determination combined with linear unmixing can be viewed as a non-orthogonal subspace projection which seeks to maximize the orthogonality of the end-member abundance maps with the constraint that the resulting abundance maps are non-negative and sum to one. The image is transformed such that the scatter of data all lie between zero and one for the contribution of a single end-member. A scatter plot of any two end-member abundance images ("unmixed band scatter plots") should form a triangle with vertices at the origin, (0,1) and (1,0).

This is analogous to the practice of "partial unmixing" used by Boardman *et al* (1995), and the "trine" visualization method used by Craig (1994). In a scatter plot of two bands, all data which has no contribution of either end-member will collapse to the origin. The scatter plot has no linear features save for the pure data along the coordinate axis. Other linear features not parallel to the x- or y-axis indicate either a missed or poorly chosen end-member.

Several unmixed band scatter plots are shown in Figure 8. The scatter of the data is generally parallel to the coordinate axis, as it should be. The scatter plots of abundance map 4 vs. abundance map 9 shows some non-parallel scatter, but the overall trend is quite good. This indicates that the overall data scatter generally lies within the simplex defined by the end-members. The resulting end-members should be more or less similar to end-members obtained through methods which do not use pure pixels, such as "minimum volume" methods (Craig, 1994). The major difference is that this method will have some pixels with negative abundance for certain end-members, seen by many researchers as undesirable. However some negative end-member abundances will occur even with perfect end-members due to noise. It is impossible to tell negative abundances due to noise from those due to poorly chosen end-members.

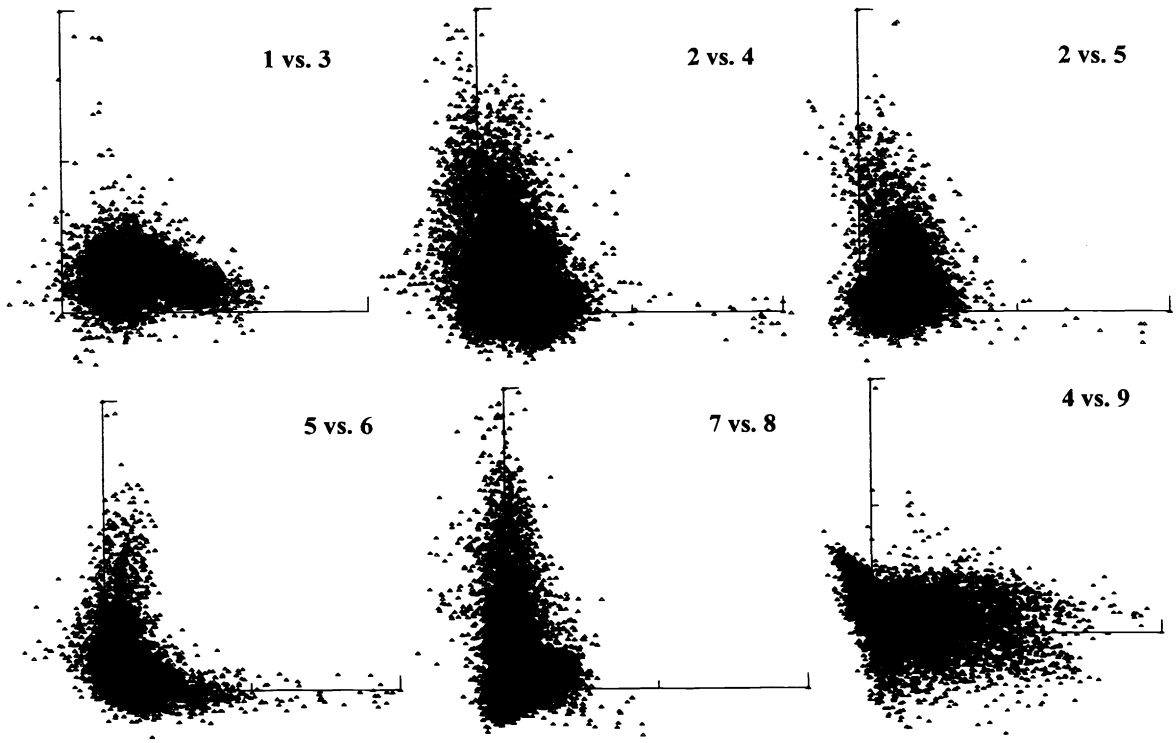

Figure 8: Scatter plots between various bands of the AVIRIS Cuprite end-member abundance images, both axis range from 0 to 1. Top row, left to right: band 1 vs. band 3, band 2 vs. band 4, band 2 vs. band 5; bottom row, left to right: band 5 vs. band 6, band 7 vs. band 8, band 4 vs. band 9.

5. CONCLUSIONS

A simple algorithm based on finding the maximum simplex that can be inscribed inside of a hyperspectral data set is capable of determining end-members in high dimensional hyperspectral images. The algorithm has been used successfully to determine end-members and unmix good quality synthetic data, and appears to be robust when used with data of poor quality. This method was used to derive end-members and end-member abundance images from a real hyperspectral data set. Derived end-members from Cuprite, Nevada AVIRIS images show a close match to USGS reference spectra (Clark, 1993), and derived abundance maps are in good agreement with those published by Resmini *et. al.* (1997).

1. Ashley, R.P., and Abrams, M. J., Alteration mapping using multispectral images, Cuprite mining district, Esmerelda County, Nevada. United States Geological Survey Open-File Report 80-367, 1980.
2. Boardman, Joseph W., "Analysis, understanding and visualization of hyperspectral data as convex sets in n-space", *SPIE Proceedings*, Vol. 2480. pp. 14-22, 1995.
3. Boardman, Joseph W., Fred A. Kruse, Robert O. Green, "Mapping Target Signatures via Partial Unmixing of AVIRIS Data", 5th Annual JPL Airborne Earth Science Workshop, Jet Propulsion Laboratory, Pasadena, CA, JPL Pub. 95-1, V.1, pp. 23-26, 1995.
4. Clark, R.N., G.A. Swayze, A.J. Gallagher, T.V. King, and W.M. Calvin, The U. S. Geological Survey, Digital Spectral Library: Version 1: 0.2 to 3.0 microns, U.S. Geological Survey Open File Report 93-592, 1340 pages, 1993.
5. Craig, M., "Unsupervised Unmixing of Remotely Sensed Images", *Proceedings of the Fifth Australasian Remote Sensing Conference*, Perth, Australia, pp. 324-330, 1990.

6. Craig, Maurice, D., "Minimum Volume Transforms for Remotely Sensed Data", *IEEE Transactions on Geoscience and Remote Sensing*, Vol. 32, pp. 542-552, 1994.
7. Green, A., M. Berman, P.Switzer, and M.D. Craig, "A Transformation for ordering Multispectral Data in Terms of Image Quality with Implications for Noise Removal, *IEEE Transactions on Geoscience and Remote Sensing*, vol. 26, no. 1, pp. 65-74, 1988.
8. Harmon, H.H., *Modern Factor Analysis*, University of Chicago Press, Chicago, 1967.
9. Ifarraguerri, Agustin and Chang, Chein-I, "Hyperspectral Image Segmentation with Convex Cones," *Proceedings of ISSSR*, 1997.
10. Lay, Steven R., *Convex Sets and Their Applications*, John Wiley and Sons, New York, 1982.
11. Lawson, Charles L., and Richard J. Hanson, *Solving Least Squares Problems*, Prentice Hall, 1974.
12. Rawlings, John O., *Applied Regression Analysis: A Research Tool*, Wadsworth & Brooks, Pacific Grove, 1988.
13. Resmini, R. G., M.E. Karpus, W.S. Aldrich, J.C. Harsanyi, M. Anderson, "Mineral mapping with Hyperspectral Digital Imagery Collection Experiment (HYDICE) sensor data at Cuprite, Nevada, U.S.A., *Int. J. Remote Sensing*, Vol. 18, pp. 1553-1570, 1997.
14. Vane, G., R. O. Green, T. G. Chrien, H. T. Enmark, E.G. Hansen, W. M. Porter, "The Airborne Visible/Infrared Imaging Spectrometer (AVIRIS)," *Remote Sensing of the Environment,* Vol. 44, pp. 127-143, 1993.
15. Winter, Michael E. "Fast Autonomous Spectral End-member Determination In Hyperspectral Data", *Proceedings of the Thirteenth International Conference on Applied Geologic Remote Sensing*, Vol. II, pp 337-344, Vancouver, B.C., Canada, 1999.